Collective Thomson scattering with 77, 154, and 300 GHz sources in LHD

M. Nishiura,[a,b,*] K. Tanaka[a], S. Kubo[a], T. Saito[c], N. Kenmochi[b], H. Nuga[a], R. Seki[a], T. Shimozuma[a], Y. Yoshimura[a], H. Igami[a], H. Takahashi[a], T. I. Tsujimura[a], R. Yanai[a], Y. Tatematsu[c], LHD Experiment Group

[a] *National Institute for Fusion Science, 322-6 Oroshi, Toki, Gifu, 509-5292 Japan*

[b] *Graduate School of Frontier Sciences, The University of Tokyo 5-1-5 Kashiwanoha, Kashiwa, Chiba, 277-8561 Japan*

[c] *Research Center for Development of Far-Infrared Region, University of Fukui 3-9-1 Bunkyo, Fukui, 910-8507 Japan*

E-mail: nishiura@nifs.ac.jp

ABSTRACT:

Collective Thomson scattering (CTS) is one of attractive diagnostics for measuring locally and directly the fuel temperature and the velocity distribution of fast ions in fusion plasmas. A mega-watt class source of millimeter or sub-millimeter waves is required to detect a weak scattered radiation superimposed on background radiation owing to electron cyclotron emissions (ECEs) from plasmas. Based on electron cyclotron resonance heating (ECRH) system with the frequencies of 77 GHz and 154 GHz in the Large Helical Device (LHD), the CTS diagnostic system has been developed to measure bulk ion temperatures from a few keV to ~10 keV and fast ions originated from 180 keV-neutral beam injection in the LHD. The measured CTS spectra and their time evolutions are analyzed with the electrostatic scattering theory. The bulk ion temperatures obtained from CTS spectra increase with the neutral beam injections and decrease with the heating terminated. The velocity map of simulated fast ions explains that the bumps on tail of measured CTS spectra are caused by the co- and counter- fast ions. A new prescription for anisotropic velocity distribution function is proposed. As for 154 GHz bands, the CTS spectrum broadenings for D and H plasmas are distinguished reasonably at the same temperature, and its ion temperatures are comparable to those of the charge exchange recombination spectroscopy. As reactor-relevant diagnostics, a 300 GHz gyrotron and a corresponding receiver system have been implemented in LHD to access high density plasmas with low background ECEs. The recent progress for CTS diagnostics and their spectrum analysis with the probe frequencies of 77 GHz, 154 GHz, and 300 GHz in the LHD experiments is described.

KEYWORDS: Collective Thomson scattering; Plasma diagnostics; Deep learning; Tomography.

[*] Corresponding author.

Contents

1. Introduction

The fusion plasma diagnostics are essential to study plasma confinement and to control burning plasmas in fusion devices. For bulk and fast ion diagnostics in fusion plasmas, a collective Thomson scattering (CTS) diagnostic system is one of the candidates for diagnosing bulk and fast ions. The CTS diagnostic enables us to measure an ion velocity distribution function in high temperature plasmas. Since the scattered radiation is small, a mega-watt class probe beam is required to realize the CTS diagnostic. Fusion devices usually equip a mega-watt gyrotron for electron cyclotron resonance heating (ECRH). Thus, the CTS diagnostics have made progress in the development and the physics research in ASDEX-UG [1], Wendelstein 7-X [2], and the Large Helical Device (LHD) [3-7] as the existing devices, and in ITER.

In the LHD, we have analyzed the time evolution of CTS spectra in 77 GHz range [6]. Neutral beam heating (NBI) originates the fast ions with anisotropic velocity distribution functions. The measured CTS spectrum becomes the projection onto the fluctuation wave vector $\boldsymbol{k}^{\delta} = \boldsymbol{k}^{s} - \boldsymbol{k}^{i}$. Here $\boldsymbol{k}^{s}$ and $\boldsymbol{k}^{i}$ are the wave vectors of the scattered radiation and the incident radiation. The reconstruction procedure is desired from the measured one dimensional velocity distribution to the velocity space (v_{para}, v_{perp}). The new procedure is proposed to reconstruct the fast ion population on (v_{para}, v_{perp}) map from the measured CTS spectra.

In this paper, we report the recent development status on CTS diagnostics in the LHD.

2. CTS diagnostics in the LHD

In the LHD, we started the development of the CTS diagnostic in 77 GHz band. Higher frequency of the probe beam is favorable for preventing the harmful effects and for extending the diagnostic performance. ECRH system in the LHD has operated 154 GHz gyrotrons, and a dedicated 300 GHz gyrotron was prepared for CTS diagnostics [8]. In the case of the higher frequency, we should take into account the CTS diagnostics. The Salpeter parameter $\alpha = 1/(|\boldsymbol{k}^{\delta}|\lambda_D)$ decreases. Here, the Debye length λ_D, the scattering angle θ between the incident wave and the scattered wave, and $|\boldsymbol{k}^{\delta}| \cong 2|\boldsymbol{k}^{i}| \sin(\theta/2)$ are used to calculate α. This leads to α close to one, which means that the ion component in the measured CTS spectrum is weaker than the electron

component. The decrease of α makes the ion measurement difficult. In addition, the signal level of scattered radiation becomes smaller. The feature is summarized in Table 1.

Three gyrotron frequencies, 77 GHz, 154 GHz, and 303 GHz (the nominal frequency is 300 GHz) can be selected for CTS diagnostics in LHD experiments. The appropriate frequency should be chosen for plasma conditions and target ions. As the electron density approaches to the cut off density of 7×10^{19} m^{-3} for the O-mode of the 77 GHz electromagnetic wave, the rays of the probe beam and the receiving beam start refracting in plasmas. The probe beam and the receiving beam in 77 GHz band are sometimes refracted in plasmas at a density regime (~ 4×10^{19} m^{-3}) [6]. Such situation makes the alignment difficult to set the scattering volume accurately. When the probe beam is aligned by scanning the receiver beam spatially, the low CTS signal still remains in some conditions at a position where the beam overlap does not exist ideally. One of the possible reasons would be a change in the beam divergence in plasma, which results in the change in the beam diameter. Even below the cutoff density, the beam ray starts the refraction. This effect is sometimes inevitable for a large scale machine. To solve the problem, the frequency of 154 GHz for a probe beam of CTS diagnostic is considered as an alternative of 77 GHz. Another candidate is the use of a 300 GHz pulse gyrotron developed at the University of Fukui [8]. They have achieved an output power higher than 300 kW with the pulse width of 30 μs. The duration is limited by the power supply. When the output power is 150 kW, the pulse width extends to 100 μs [9]. In addition, compared with the merit of using the frequency of 154 GHz, a 300 GHz CTS diagnostic has the advantage of the geometrical limitation, because the frequency of 300 GHz is free from fundamental and second harmonic electron cyclotron resonances in plasmas.

Figure 1 shows the calculated CTS spectra for the probe beam frequencies of 77 GHz, 154 GHz, and 300 GHz with the same plasma parameters to understand the characteristics of the CTS spectra. The overlap position is set to the local coordinate at the 2-O port, (R, T, Z) = (3.673, 0.4 , 0) for all cases. The probe beam and the receiving beam use the 2O-LR antenna and the 2O-LL antenna, respectively. The angle θ is set to 169 degrees near the back scattering geometry. The CTS spectrum features are summarized in Table 1. When the probe frequency is higher, the intensity of scattered radiation decreases. This is a demerit in terms of the signal to noise ratio. The factors in this frequency region are at most 1/10 times for 154 GHz and 1/100 times for 300 GHz, respectively. The spectrum broadening increases as the probe frequency becomes higher. When the frequency of the probe beam is lower, the measurement of the ion temperature might be severe, because the bandwidth of a notch filter in the receiver is approximately a few hundred MHz. In addition, the CTS spectrum in the bulk part is affected by the fast ion component. The effect makes the spectrum analysis difficult. The Salpeter parameter α for 300 GHz still satisfies more than unity. When α for 77 GHz is ~ 5 and larger, the fast ion diagnostic becomes possible. The intermediate frequency of 154 GHz gives the small signal for fast ions in the range of 1.2 GHz in the total CTS spectrum. These characteristics of CTS spectra should be taken into account for in the bulk and fast ion measurements.

Table 1. The features of CTS spectrum for the probe beam frequencies of 77 GHz, 154 GHz, and 303 GHz.

Probe frequency	77 GHz	154 GHz	303 GHz
Scattered radiation	high	⟶	low
Spectrum broadening	narrow	⟶	wide
Salpeter parameter α	~ 5	~ 2.5	~ 1.3
Ion temperature measurement	possible	possible	possible
Fast ion measurement	possible	not possible	not possible

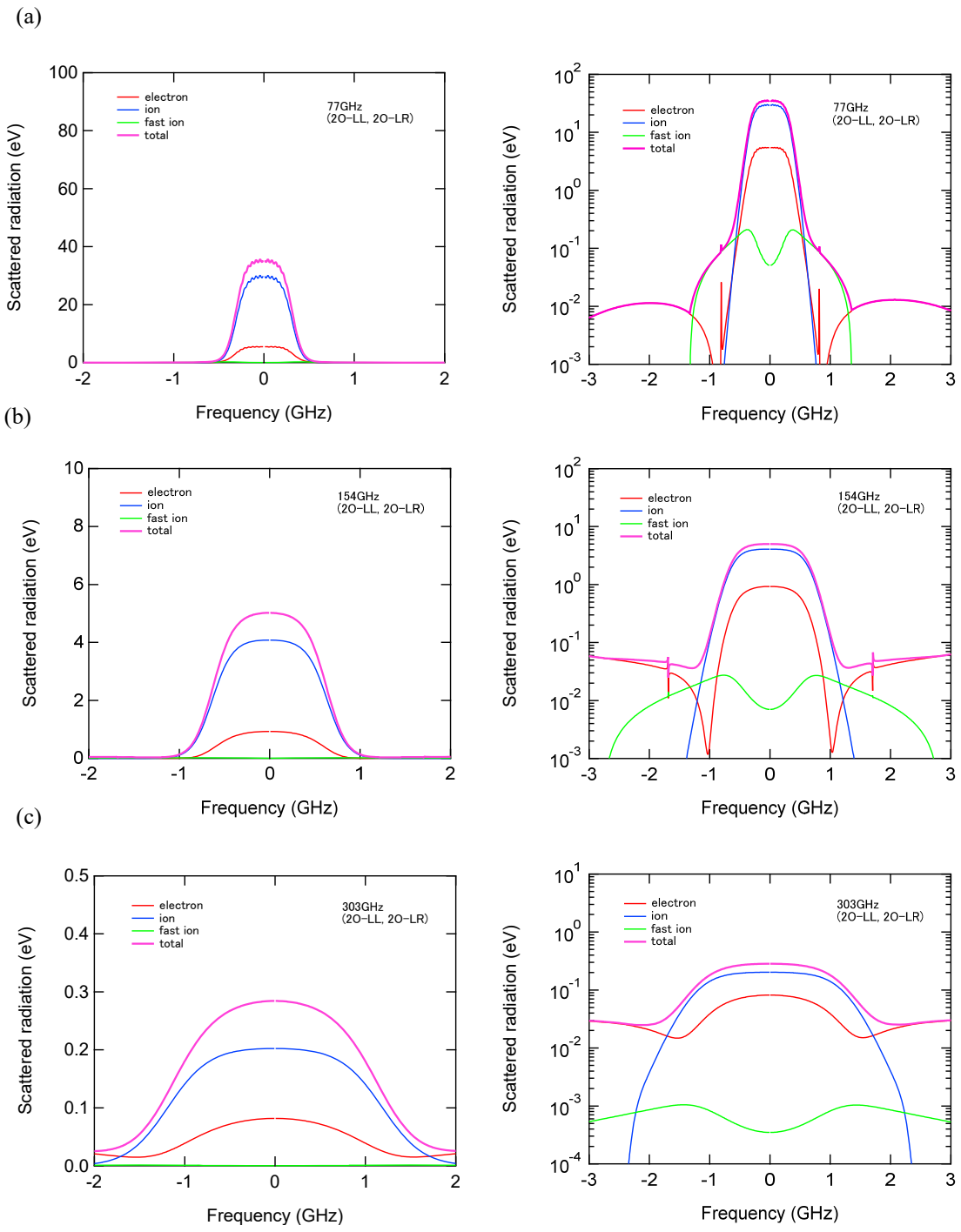

Figure 1: Calculated CTS spectra (blue: ion, red: electron, green; fast ion, pink: sum of three particles) at the frequencies of (a) 77GHz O-mode, (b) 154 GHz X-mode, and (c) 300 GHz X-mode for probe beam and receiving beam. Figures on the right are the logarithm scale to show the fast ion component. The plasma parameters are set to $n_e = 1.5\times10^{19}$ m^{-3}, $n_i = 1.5\times10^{19}$ m^{-3}, $n_{fast} = 1\times10^{17}$ m^{-3}, $T_e = 1$ keV, $T_i = 1$ keV, $T_{fast} = 40$ keV. The LHD magnetic field on the plasma axis is set to $B_t = 2.75$ T. The angle θ is 169 degrees.

3. Experimental setup of CTS diagnostic system in the LHD

The LHD has implemented five gyrotrons connected to their transmission lines for ECRH. Three of the mega-watt class gyrotrons are the frequency of 77 GHz, and the other two gyrotrons are the frequency of 154 GHz. The 3.5 inch corrugated waveguide system transmitts electromagnetic waves from the gyrotrons. The output power for each gyrotron achieves more than 1 MW for 3 s [10]. Figure 2 shows the top view of the LHD and the port locations for the CTS diagnostic. The steering mirror is located at each exit of the transmission lines in the LHD vacuum vessel. The mirror is designed by a quasi optical system, and sets the target position of the beam for each transmission line on a shot by shot basis. Some of the steering mirrors have been improved to realize the fast motion during plasma discharges by replacing an ultrasonic motor with a servo motor [11]. The improvement of ECRH antenna system makes the LHD plasma experiments diverse. The CTS receiver uses the transmission line. The scattered radiation is collected by the mirror of the ECRH system, and is introduced into the CTS receiver. The waveguide switch is inserted in between corrugated waveguides in the transmission line, and can select the wave propagation to the gyrotron or the CTS receiver.

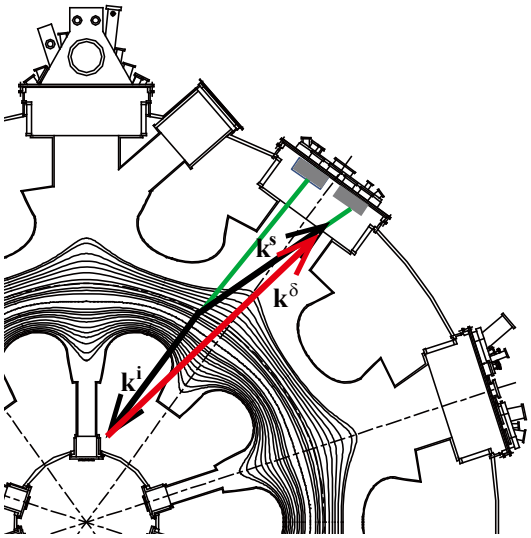

Figure 2: Top view of the LHD and the geometry of probe beam and receiving beam.

Four transmission lines of ECRH are concentrated on 2-O port of the LHD vacuum vessel. Two of these transmission lines are used for CTS diagnostic. The probe beam for 77 GHz and 154 GHz each uses the port of 2O-LR and 2O-UL, respectively. The receiving beam uses the port of 2O-LL for both frequencies. The 300 GHz system shares the transmission line at the port of 2O-UL.

The CTS receiver consists of radio frequency (RF) and intermediate frequency (IF) parts, as shown in the figure 3. The IF part is divided into the filter bank receiver and the fast sampling digitizer. The filter bank receiver divides the IF signal into 32 channels for fast ions and 8 channels for bulk ions [6], and into a high sampling digitizer. For the probe frequencies of 77 GHz and 154 GHz, the IF signal is detected by common components. We assembled newly the RF part for 300 GHz CTS diagnostic. Depending on the frequency of the probe beam, the RF part is replaced by the dedicated notch filter and the mixer.

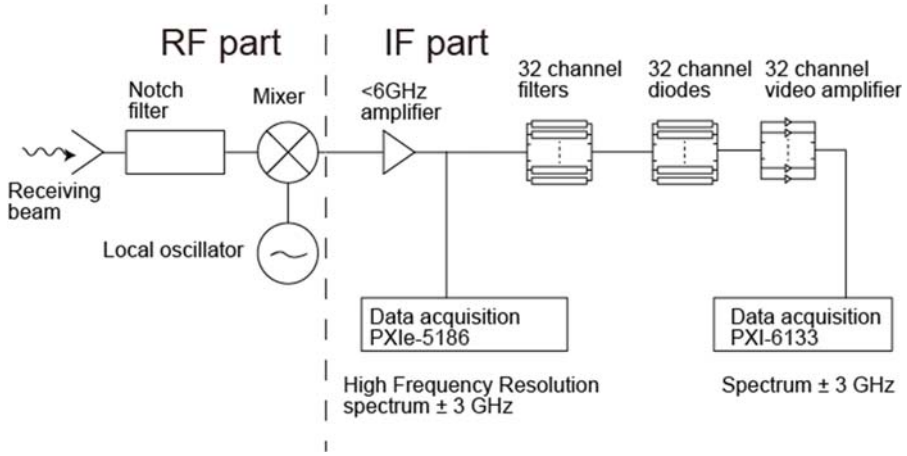

Figure 3: Diagram of the CTS receiver. RF part is replaced in accordance with the probe frequency.

4. Status of 300 GHz CTS system

We have prepared the 300 GHz CTS system. The 300 GHz gyrotron was implemented in the gyrotron room of the LHD, and was connected to one of the transmission lines using the waveguide switch. The 3.5 inch corrugated waveguide is used in the transmission lines for ECRH system. The beam profile was measured at the exit of the 300 GHz gyrotron and the 2-O port to evaluate the transmission efficiency. We found that the efficiency at 300 GHz radiation is 40 % at the injection port. The efficiency can be increased by improving the misalignment of the waveguide switch for merging the 300 GHz wave from the gyrotron to the corrugated waveguide in the transmission line. This problem will be fixed by adjusting the axis of the waveguide switch.

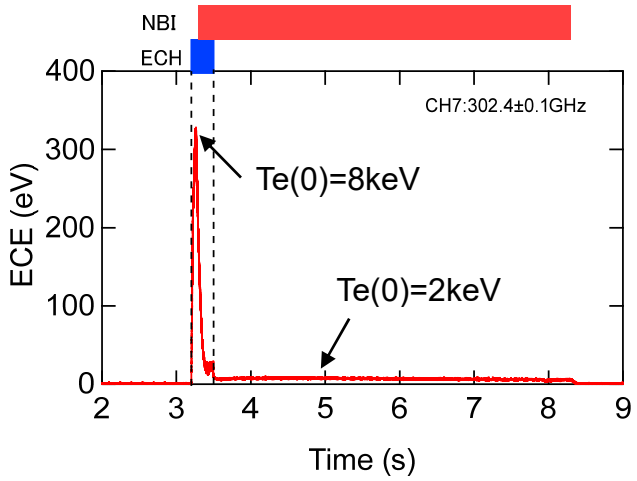

Figure 4: ECE signal for LHD shot#152391. Te(0) indicates the central electron temperature measured by the incoherent Thomson scattering.

The CTS receiver for 300 GHz was tested during the LHD plasma discharge. The magnetic configuration was R_{ax} = 3.75 m and B_t = 2.64 T. The plasma discharge started at 3.3 s by the ECRH. The NBI sustained the plasma discharge with the central electron density $n_e(0)=5\times10^{19}$ m^{-3}. As shown in the figure 4, the ECE signal in the filter bank receiver was detected successfully. The channel #7 measured the radiation at the center frequency of 302.4 GHz with the bandwidth of 0.2 GHz.

5. Analysis of CTS spectrum for bulk and fast ion diagnostics

When the charged particles have anisotropic velocity disbribution functions, the inversion problem of the measured CTS spectrum should be solved to reconstruct the velocity space (v_{para}, v_{perp}). This problem is discussed in references [12, 13]. Salewski *et al*. introduced the new idea of reconstruction prescription to the multi views of diagnostic systems. To analyze the measured CTS spectra, a new inversion method with the deep learning is introduced. The reconstruction procedure has already been demonstrated in solving the coherence imaging spectroscopy (CIS) [14]. The CIS measured the projection quantity onto the line of sight. Salewski *et al*. obtained the local profile on the poloidal plane from the CIS data using the new method. Figure 5 show the model function of fast ion population, the projection function g(u), and the reconstructed population. The measurement view of the CTS diagnostic is directed to $\boldsymbol{k}^{\delta}$ on the velocity space. The model population places on the grids of 127 × 64. The angle of $\angle(\boldsymbol{B}, \boldsymbol{k}^{\delta})$ is defined as ϕ. After the relation between the model data and the projection function g(u) for two views at ϕ = 10 and 103 degrees is learned

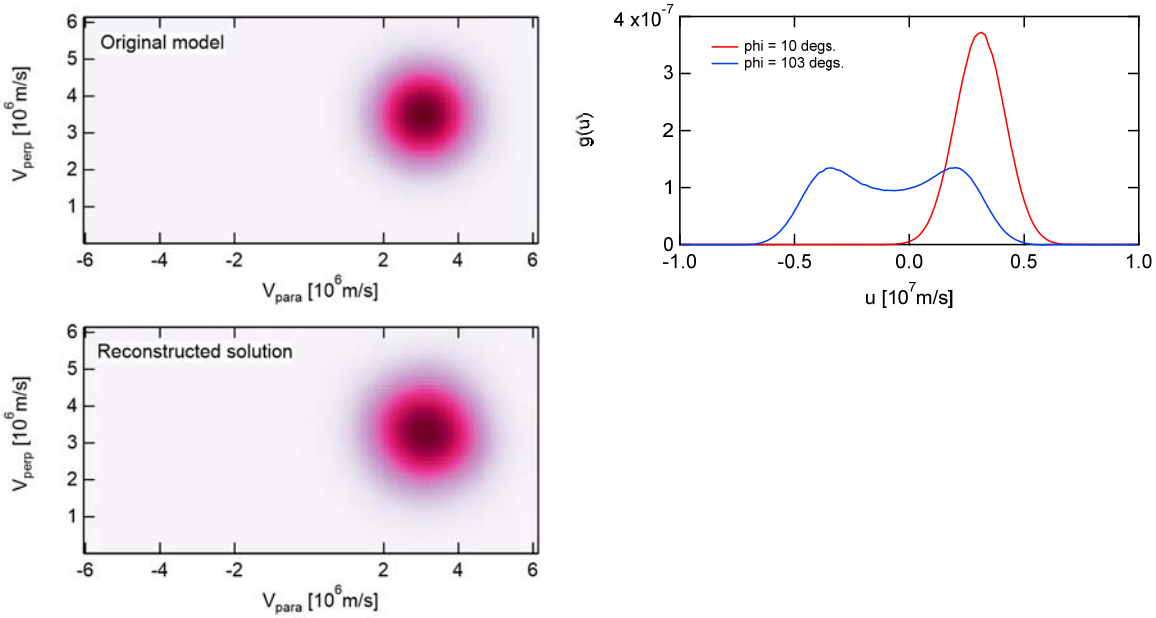

Figure 5: fast ion population on the velocity space. Original distribution (upper left). The projection g(u) in two views with ϕ = 10 and 103 degrees (right). Reconstructed population from g(u) (lower left).

in 8128 model cases, the velocity distribution function is reconstructed as shown in figure 5. Table 2 shows the numerical indices for the reconstructed result. The indices of structural similarity (SSIM), normalized root-mean-square error (NRMSE), and peak signal-to-noise ratio (PSNR) reflect the resemblance to the original velocity distribution function.

Table 2. Numerical indices of fast ion model.

	Mean	Standard deviation
SSIM	0.976	0.0057
NRMSE	0.049	0.0135
PSNR [dB]	28.10	2.6334

The test case gives us the reasonable reconstruction for the simple population function. This new procedure for velocity space tomography will be applied to more realistic population functions, and the reconstruction results will be validated.

References

[1] S. K. Nielsen *et al*., Plasma Phys. Control. Fusion **57** 035009 (2015).

[2] D. Moseev *et al*., Review of Scientific Instruments **90** 013503(2019).

[3] S. Kubo *et al*., Review of Scientific Instruments **81** 10D535 (2010).

[4] M. Nishiura *et al*., Review of Scientific Instruments **79** 10E731 (2008).

[5] Masaki Nishiura *et al*. Plasma and Fusion Res. **8**, 2402027 (2013).

[6] M. Nishiura *et al*. Nuclear Fusion **54**, 023006 (2014).

[7] K. Tanaka *et al*., Journal of Instrumentation **13**, C01010 (2018).

[8] T. Saito *et al*., Plasma and Fusion Research **12**, 1206013 (2017).

[9] T. Saito *et al*., Plasma and Fusion Research 14, 1406104 (2019).

[10] H. Takahashi *et al*., Nuclear Fusion **53**, 073034 (2013).

[11] K. Okada *et al*., Review of Scientific Instruments **85** 11E811 (2014).

[12] M. Salewski *et al*., Nuclear Fusion **51**, 083014 (2011).

[13] M. Salewski *et al*., Nuclear Fusion **52**, 103008 (2012).

[14] N. Kenmochi *et al*., Plasma and Fusion Research: Rapid Communications **14** 1202117 (2019) .